Remote Sensing of Environment 317 (2025) 114528

Contents lists available at ScienceDirect

Remote Sensing of Environment

journal homepage: www.elsevier.com/locate/rse

Measuring topographic change after volcanic eruptions using multistatic SAR satellites: Simulations in preparation for ESA's Harmony mission

Odysseas Pappas [a,b,*], Juliet Biggs [b], Pau Prats-Iraola [c], Andrea Pulella [c], Adam Stinton [d,e], Alin Achim [a]

[a] Visual Information Laboratory, University of Bristol, 1 Cathedral Square, Bristol, BS1 5TE, UK
[b] School of Earth Sciences, University of Bristol, Queens Road, Bristol, BS8 1RJ, UK
[c] Microwaves and Radar Institute, German Aerospace Center (DLR), Munchener Straße 20, Weßling, 82234, Germany
[d] Montserrat Volcano Observatory, Flemmings, Montserrat
[e] Seismic Research Centre, University of the West Indies, St Augustine, Trinidad & Tobago

ARTICLE INFO

Edited by Jing M. Chen

Keywords:
Synthetic aperture radar
Bistatic inSAR
ESA Harmony
Volcanoes
Lava flows

ABSTRACT

Volcanoes are dynamic systems whose surfaces constantly evolve. During volcanic eruptions, which can pose great threat to local communities, significant changes to the local topography occur as edifices build up and/or collapse and lava, tephra and other eruptive products are deposited. Monitoring such changes in topography is crucial to risk assessment and the prediction of further eruptive behaviour. Multistatic Interferometric Synthetic Aperture Radar (InSAR) is a remote sensing modality particularly suited to this task as it allows for the creation of digital elevation models (DEMs) that can accurately map out three-dimensional changes in the topography, regardless of weather conditions and temporal decorrelation caused by volcanic activity. Few such missions are however currently operational. Harmony is an upcoming ESA mission that will be operating alongside Sentinel-1 and will provide multistatic InSAR capabilities for the measurement of stress and deformation across the cryosphere, the oceans and the solid earth, with the monitoring of topographic change due to volcanic eruptions being one of the specific areas of focus for the mission.

In this work we demonstrate the use of high resolution bistatic interferometric data from TanDEM-X for the measurement of topographic change after recent eruptions in El Reventador, Ecuador and La Soufrière, St. Vincent and the Grenadines. Additionally, we simulate data at the lower, 20 m resolution of Harmony so as to gain insights into its capability in quantifying topographic change. Our results demonstrate that Harmony's resolution can be sufficient to resolve and measure accurately topographic change such as the emplacement of lava flows, but may be challenged in areas of steep topography where unwrapping errors can occur. The experimental results highlight the effect of acquisition pass direction with respect to local topography, the challenges arising in areas of steep topography and the importance of masking results based on estimates of precision and resolution. Finally we discuss some of the challenges, as well as implications of the Harmony mission for the future of volcano monitoring.

1. Introduction

Volcanic eruptions are amongst the most dangerous natural hazards, posing severe potential threat to human life as well as long-lasting averse economic impact to local communities. Volcanoes are dynamic systems and their surfaces are constantly evolving through time due to magmatic processes (e.g. propagation of an intrusion, emplacement of volcanic flows, dome growth) and external forcing (e.g. gravity, erosion, climate) (Loughlin et al., 2015). Each eruption builds the edifice with the accumulation of volcanic deposits whereas collapse events have the potential to suddenly destroy a large portion of the built relief (McGuire, 1996; Eiden et al., 2023). Both construction and collapse pose a significant hazard to the surrounding areas, as illustrated by fatalities caused by collapses at Merapi (2010); Fuego (2018); Anak Krakatau (2018) and Hunga-Tonga (2022) and destruction associated with lava flows at Kilauea (2018) and Cumbre Vieja (2021). Over 800 million people across the world live within 100 km of a volcano — yet despite population growth, the number of fatalities per eruption has declined rapidly thanks to improved monitoring, hazard assessment, awareness and communication (Loughlin et al., 2015). Maps of surface displacement and topographic change are vital for understanding the

* Correspondence to: Visual Information Laboratory, School of Computer Science, Merchant Venturers Building, 75 Woodland Road, Bristol, BS8 1UB, UK.
E-mail address: o.pappas@bristol.ac.uk (O. Pappas).

https://doi.org/10.1016/j.rse.2024.114528
Received 24 June 2024; Received in revised form 16 October 2024; Accepted 18 November 2024
Available online 29 November 2024

geometry and activity of underlying magma storage areas and the stability of steep volcanic edifices (Eiden et al., 2023; Biggs and Wright, 2020; Poland and Zebker, 2022).

Although field measurements (GNSS, levelling) can be used to measure topographic changes, the most significant changes typically occur in steep slopes and/or hazardous locations where the installation of ground instrumentation is nearly impossible and poor spatial and temporal resolution limits the retrieval of erupted volumes. Since the late 1990's, it has been possible to construct DEMs of volcanoes using satellite data from either optical (e.g. SPOT, ASTER Abrams et al., 2010, and more recently, high-resolution 2 m WorldView and GeoEye data as used in the Polar Geospatial Center's EarthDEM (Porter et al., 2022) and ArcticDEM Porter et al., 2023) or radar (SRTM Farr et al., 2007) imagery (e.g. Chorowicz et al., 1992; Mouginis-Mark et al., 2001; Kervyn et al., 2008). However, in volcanic environments, the recurrent presence of clouds or eruption plumes around the summit limits the use of optical data.

Interferometric Synthetic Aperture Radar (InSAR) is better suited to retrieve topographic changes in volcanic environments as it performs measurements at day and night for all weather conditions. While a number of SAR satellites can be used to form repeat-pass interferograms from which topographic change can be evaluated (e.g. Naranjo et al., 2016; Ebmeier et al., 2012), single-pass bistatic SAR missions such as TanDEM-X (Krieger et al., 2007) offer distinct performance advantages towards the formation of accurate, high resolution DEMs (Kubanek et al., 2021). As the pair of images that form the interferometric pair are acquired at the same time, they do not suffer from loss of coherence due to temporal decorrelation to the same extent as repeat-pass acquisitions. Atmospheric correction, a crucial step for repeat-pass interferometry, is also not required in the case of bistatic SAR. However, few such satellite missions are currently operational, with limited spatial and temporal coverage (in terms of low-level data availability) compared to repeat-pass InSAR data (Kubanek et al., 2021). Bistatic TanDEM-X (TDX) has been widely used in mapping out topographic changes at volcanoes (Pritchard et al., 2018; Galetto et al., 2024). This includes lava flows fields at Kilauea, Hawaii (Poland, 2014), Reventador, Ecuador (Arnold et al., 2017, 2019), Nyamuragira, DRC (Albino et al., 2015), Tolbachik, Russia (Kubanek et al., 2015a) and Bardarbunga, Iceland (Dirscherl and Rossi, 2018). TanDEM-X has also been used to provide a snap-shot of dome growth and collapse at Merapi, Indonesia (Kubanek et al., 2015b; Grémion et al., 2023) and of the erosion and deposition associated with a pyroclastic flow at Fuego, Guatemala (Albino et al., 2020). However, the limited acquisitions of TanDEM-X has made measuring topographic change associated with more rapid and unpredictable events challenging.

Besides TDX, which is arguably the most widely used source of bistatic InSAR data currently, operators of private SAR constellations UMBRA and Capella Space have both recently demonstrated multistatic InSAR capabilities with their satellites, while ICEYE and SATLANTIS are jointly planning a new constellation for this purpose. These newer generation satellites provide increased spatial resolutions, with UMBRA spotlight data for example at an impressive 50 cm, and have the potential to provide very extensive spatiotemporal coverage due to their populous constellations. Data availability from these missions is however limited as of this time, especially non-commercially, and this in turn severely limits their current use for volcano monitoring. Some products are made available for research purposes via programmes such as ESA's Third Party Missions, CEOS and UMBRA's Open Data programmes; these collections however rarely include bistatic interferometric image pairs.

In 2022, the European Space Agency (ESA) confirmed that 'Harmony' will be the 10th Earth Explorer Mission, scheduled for launch in 2029. Harmony will consist of two satellites, each carrying as main payload a passive, receive-only synthetic aperture radar (SAR) and operating in a constellation with Sentinel-1, providing a dense time-series of surface elevation models at a temporal interval of 12 days.

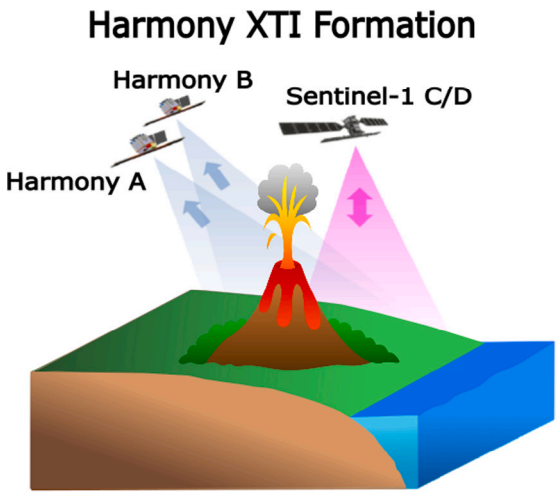

Fig. 1. Harmony XTI operational configuration. XTI formation allows the retrieval of dense time series of surface elevation models while retaining 3D InSAR capabilities. *Source:* Modified from Lopez-Dekker et al. (2021).

Measuring topographic change over time will provide new constraints on eruption rates which can be used to forecast the behaviour of an ongoing eruption. Updated DEM information can be used to measure the growth and collapse of volcanic domes and improve modelling of the potential paths and inundation areas of hazardous mass flows (primarily lava, pyroclastic density currents, and lahars).

In this study, we assess the ability of Harmony to measure topographic change in volcanic conditions. We consider two end-member styles of eruption — the 2011–2014 phase of the effusive eruption of El Reventador, Ecuador, and the 2021 explosive eruption of La Soufrière, St Vincent and consider the challenges posed by steep volcanic terrain. First we produce topographic change maps using high-resolution bistatic data provided by TanDEM-X. We then subsample the TanDEM-X data to a spatial resolution matching the expected resolution of Harmony and reprocess to produce topographic change maps at Harmony's spatial resolution. The remainder of this article is structured as follows: Section 2 provides background information on the ESA Harmony mission, its application to monitoring volcanic topographic change and the eruption case studies of El Reventador and La Soufrière, St Vincent. Section 3 outlines the processing methodology for the experiments for both high-resolution and subsampled data, with results for both case studies presented in Section 4. Section 5 provides discussion points on the challenges of InSAR volcano monitoring, as well as on the implications and future benefits Harmony will have in this context.

2. Background

2.1. The Harmony mission

Harmony is an upcoming Earth Observation satellite mission by the European Space Agency. It has been selected as the 10th Earth Explorer mission in ESA's FutureEO programme, with a launch date scheduled for 2029 (ESA Harmony Mission Advisory Group, 2022). Harmony will be dedicated to the observation and quantification of small-scale deformation, seeking to answer scientific questions related to ocean, ice and land dynamics. These include the measurement and tracking of air-sea boundary interactions and their effect on tropical storm formations, the measurement of glacier dynamics and glacier/ice-sheet mass balance, the measurement of 3-D surface motion in tectonic regions and finally the evaluation of topographic change related to volcanic eruptions (Lopez-Dekker et al., 2021).

The mission will consist of two satellites, each equipped with passive, receive-only SAR instruments as well as a thermal infra-red instrument. These two satellites will operate in convoy with one of the Sentinel-1 satellites, which will serve as the SAR transmitter of opportunity, in two different formations, allowing for two different modes of observation. In StereoSAR mode, the Harmony satellites will be flying ahead of and behind Sentinel-1, providing high resolution measurements of surface roughness to retrieve high resolution surface stress-equivalent winds and surface currents over sea, complemented by observations of sea-surface temperature and cloud motion provided via the thermal infra-red instrument. Over land, the line-of-sight diversity afforded in this formation will allow the retrieval of 3-D surface motion vectors. In the across-track interferometry (XTI) configuration, illustrated in Fig. 1, the two Harmony satellites will be flying in a passively safe helix formation with Sentinel-1 and provide a dense time series of surface elevation models at a temporal interval of 12 days.

Performance requirements for the Harmony topographic change (TOC) products are a 20m spatial resolution, and a 1.5 m vertical measurement accuracy, as outlined in the Mission Requirements Document (ESA Earth and Mission Science Division, 2023). It is worth noting that the perpendicular baseline between the two Harmony satellites in XTI mode will vary with latitude across orbit — this would affect to some extent the Height of Ambiguity and vertical accuracy with which different areas of the Earth would be imaged. Exact baseline values are to be determined at a later stage of mission design, they are however expected to vary from 500 to 800 meters across orbit (Hooper et al., 2019).

Harmony's time series of DEMs will be of great value to many applications, including the evaluation of topographic change resulting from volcanic eruptions. Retrospective analysis of eruptions between 1980 and 2019 show that topographic change data with a 13 m spatial resolution would have been sufficient to detect 90% of all volcanic eruptive products and a 1 m vertical accuracy would detect 92% of all eruptive (Eiden et al., 2023). While Harmony's envisaged resolution and accuracy do not quite match these ideal requirements, they do provide as close an approximation as feasible, especially given the constraints imposed by operating in conjunction with the Sentinel-1 platform.

Harmony is currently planned to have a 5 year mission lifetime, with the Harmony satellites operating in XTI formation for years 1 & 5 and in StereoSAR for years 2, 3 & 4. Current mission plans include the provision for occasional XTI acquisitions during years 2, 3 & 4, but the exact details have yet to be decided. As an Earth Explorer, Harmony is designed to explore a wide gamut of scientific topics and must balance the requirements of each user community.

2.2. Case study eruptions

For the purposes of this study, we have used high-resolution InSAR data to evaluate topographic change for two case studies; the 2011–2014 phase of the ongoing effusive eruption of El Reventador, Ecuador, and the explosive 2020–2021 eruption of La Soufrière St. Vincent, St. Vincent and the Grenadines. These two examples present significantly different monitoring scenarios, both in terms of the mechanisms and types of topographic change, and also the local topography and hence radar imaging geometry.

El Reventador is an active stratovolcano located approximately 90 km east of Quito, Ecuador. On November 3, 2002, El Reventador volcano experienced the largest eruption in Ecuador in the last 140 years and has been continuously active ever since with both explosive and effusive activity, characterised by Strombolian and Vulcanian behaviour (Vallejo et al., 2023). Here we focus on the time period between September 2011 and June 2014, previously analysed by Arnold et al. (2017, 2019). During this period, the average elevation of the summit lava dome increased by 24 ± 4 m, while the talus deposits increased in mean thickness by 59 ± 11 m west of the dome and 39 ± 2 m to the east (Arnold et al., 2017). Lava flow extrusion between February 2012 and June 2014 produced 21 distinct lava flows described in Arnold et al. (2019) with total surface elevation changes of up to 80 m and a cumulative bulk volume difference of 33.3M ± 1.5M m^3 (26.7M ± 1.2M m^3 Dense Rock Equivalent) (Arnold et al., 2017). The area of interest around El Reventador is shown in Fig. 2(b), along with a hillshaded SRTM DEM view with the 2002–2009 and 2011–2016 lava flow fields demarcated.

La Soufrière, St. Vincent, is an active stratovolcano located on the northern part of the island of St. Vincent in St. Vincent and the Grenadines. A major eruption in 1979 created a lava dome within the crater with a diameter of 868 m, a height of 133 m and total volume of 50×10^6 m^3 (Fiske and Sigurdsson, 1982; Shepherd et al., 1979). La Soufrière, St. Vincent's most recent eruption began on December 27, 2020 and was characterised by increased seismicity and the growth of a new lava dome on the south-western edge of the main crater (Global Volcanism Program, 2021; Joseph et al., 2022; Stinton, 2024). The effusive eruption continued throughout the following months, with the newly formed lava dome growing to 105 m tall, 243 m wide and 921 m long by 19 March 2021 (Stinton, 2024). An average extrusion rate of 1.8 m^3 s^{-1} between December 2020 and March 2021 has been reported for this effusive eruption phase, with total extruded volumes of lava reported varyingly from 16 to 19.4 million m^3 (Dualeh et al., 2023a; Stinton, 2024). On the morning of the 9th April 2021 (one day after the local authorities declared a red alert and issued an evacuation order for the area) an explosive eruption occurred, with an ash plume reaching 8000 m in altitude and drifting eastward. Explosions continued over the following days. By the end of the explosive eruptive phase the topography around the volcano crater had been significantly altered. The new lava dome formed during the effusive stage of the eruption, as well as the pre-existing 1979 lava dome were completely destroyed. A new crater, about 900 m in diameter and at least 100 m deep, was formed with tephra deposited along its eastern semicircle (Global Volcanism Program, 2021). The area of interest around La Soufrière, St. Vincent is shown in Fig. 2, along with hillshaded high-resolution Pléiades 2 m DEM (Fig. 2(c)) and SRTM 30 m DEM (Fig. 2(d)) views, with the new crater and tephra deposit fields demarcated.

For both volcanoes of interest, we have demarcated a small, relatively flat reference area where little to no topographic change is expected to be found. This will serve as a later stage to quantify uncertainty in our measurements of topographic change, following the methodology of Kubanek et al. (2017) and Albino et al. (2020). These areas are shown in the red dashed-line rectangles in Fig. 2(b), (c) and (d).

3. Methodology

3.1. Dataset

We use high-resolution bistatic InSAR data from TanDEM-X (TDX) provided by the German Aerospace Center (DLR), as part of the Committee on Earth Observation Satellites (CEOS) Volcano Pilot project (Pritchard et al., 2018). Interferometric image pairs are provided in the form of co-registered, single-look, slant range complex imagery (TanDEM-X Coregistered Single-look Slant range Complex (CoSSC) products) at a spatial resolution of ≈ 3 m for Stripmap acquisitions. Note that spatial resolution differs from pixel spacing, with the latter being approximately 1 m in range and 2 m in azimuth for our TDX products. Further technical specifications of the available TanDEM-X CoSSC products can be found in Table 1.

For El Reventador, our catalog contains 4 Stripmap products from the ascending pass orbit that had previously been analysed by Arnold et al. (2017), spanning from September 2011 to June 2014. We focus on the data from September 2011, which allow for an evaluation of the lava flow field from 2002–2009 (Naranjo et al., 2016) and the data from June 2014, which allows for the evaluation of the (ongoing at the

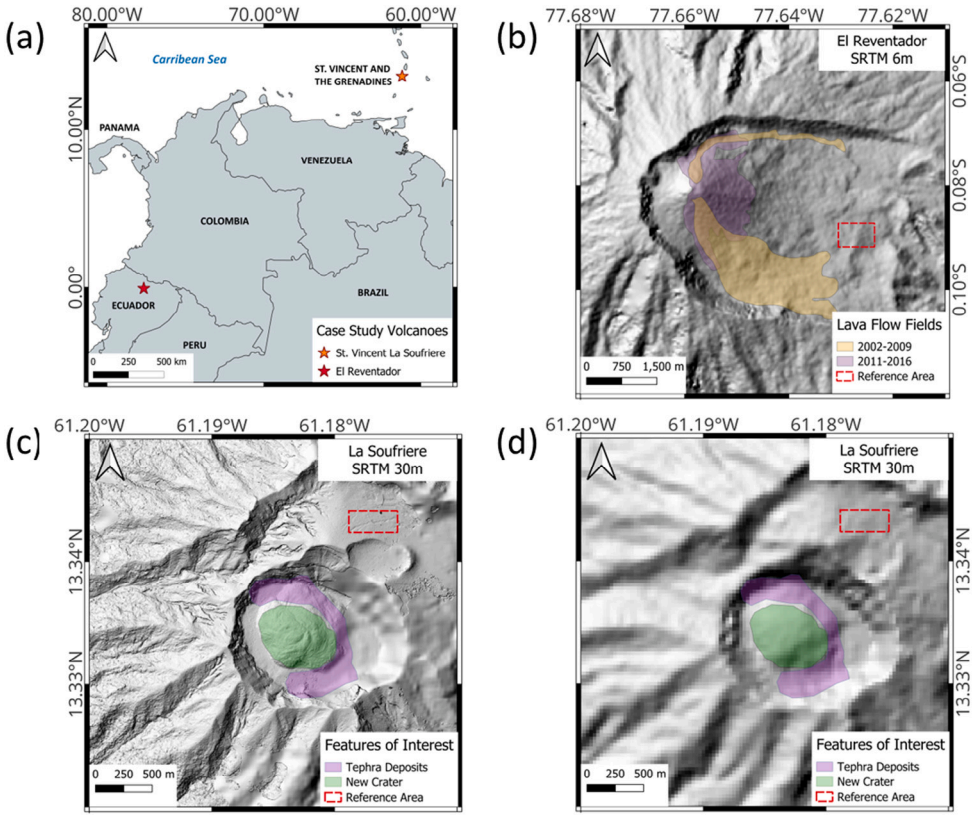

Fig. 2. (a) Geographic location of El Reventador, Ecuador and La Soufrière, St. Vincent, St. Vincent and the Grenadines. (b) SRTM 6 m upsampled DEM for El Reventador. (c) Pléiades 2 m DEM for La Soufrière, St. Vincent (Grandin and Delorme, 2021). (d) SRTM 30 m DEM for La Soufrière, St. Vincent. Pléiades data acquired in 2014, SRTM acquired in 2000. Features of interest demarcated on the DEMs.

Table 1
TanDEM-X CoSSC product parameters for case study eruptions at El Reventador, Ecuador & La Soufrière, St Vincent.

	Date	Pass	Heading	Inc. Angle	Range spacing	Az. Spacing	Baseline
Reventador D1	09/09/2011	Ascending	349°	38.2°	0.91 m	2.22 m	124 m
Reventador D2	24/07/2012	Ascending	349°	38.3°	1.36 m	2.22 m	233 m
Reventador D3	11/07/2013	Ascending	349°	38.3°	1.36 m	2.22 m	102 m
Reventador D4	06/06/2014	Ascending	349°	38.3°	1.36 m	2.22 m	150 m
La Soufrière D1	17/01/2017	Ascending	349°	33.6°	1.36 m	1.97 m	110 m
La Soufrière D2	26/05/2019	Descending	190°	46.2°	1.36 m	2.17 m	196 m
La Soufrière D3	10/10/2021	Ascending	349°	34.7°	0.91 m	1.97 m	176 m

time) 2011–2016 lava flow field (Arnold et al., 2017). For La Soufrière, St. Vincent, two pre-eruptive Stripmap acquisitions were available in the catalog, namely an ascending pass acquisition in January 2017 and a descending pass acquisition in May 2019. However, only one post-eruptive acquisition was available, acquired in October 2021 from an ascending track. Unfortunately, no data acquisitions during the lava dome growth phase were available, nor were any descending-pass post-eruptive acquisitions. As a result, we are limited to the evaluation of the final topographic change after the end of both effusive and explosive phases of the eruption.

Pre-eruptive DEMs are critical for the evaluation of topographic change via InSAR as they allow for the simulation of the pre-existing topographic phase and subsequent removal thereof from the measured interferogram; this is crucial in facilitating successful unwrapping of the interferograms in areas of steep topography. DEMs can be acquired from a number of standard global coverage datasets such as SRTM/NASADEM (Farr et al., 2007) and Copernicus (ESA, 2019). SRTM data was collected during the shuttle mission in 2000, and no other major eruptions occurred at El Reventador or La Soufrière, St Vincent between this date and the observation periods of interest, making it suitable as a pre-eruptive reference DEM in both cases. However, the (usual) 30 m pixel spacing of these products is significantly larger than that of the TanDEM-X products, limiting the resolution of the topographic change map. For the case of La Soufrière, St. Vincent, a high resolution pre-eruptive DEM was available, created using Pléiades optical imagery acquired in 2014 and downsampled to a 2 m resolution (from the original 0.5 m acquisitions) (Grandin and Delorme, 2021). Gaps due to cloud cover were filled in via Copernicus 30 m data upsampled to 2 m spatial resolution. For El Reventador, no higher resolution product is available, so we follow the approach of Arnold et al. (2017), who linearly upsampled the 30 m SRTM DEM to a 6 m spatial resolution. They reported no artefacts in the topographic phase due to this oversampling.

Finally, we compare our measurements of topographic change to existing ground truth measurements collected by complementary techniques. At El Reventador, Naranjo et al. (2016) combined aerial and satellite (ASTER) imagery with field measurement to provide planimetric estimates of lava volume for 2002–2009. Arnold et al. (2017) used SAR methods to study the 2011–2016 lava flows using the same bistatic TDX InSAR data presented here and compared it to independent measurements created using radar shadowing in SAR (RADARSAT-2)

amplitude images. Finally (Vallejo et al., 2023) used aerial photogrammetry from 11 overflights in 2005–2022 to provide measurements of topographic change around the summit of the volcano.

For the case of La Soufrière, St. Vincent, Dualeh et al. (2023b) used SAR backscatter to estimate the dome volume during the effusive phase, but this technique cannot be applied to the explosive phase. The Montserrat Volcano Observatory produced topographic change maps spanning the entire eruption using aerial photogrammetry (Stinton, 2024). A post-eruption DEM of the new crater at La Soufriere, St Vincent was constructed using near vertical and oblique aerial photography. Images were collected using a Sony a6000 digital camera attached to the underside of a helicopter in a custom housing. The camera was programmed to acquire images at one second intervals in order to maximise coverage due to the presence of gas, steam and atmospheric clouds in the crater. A Garmin 64GPSmap handheld GPS device, placed inside the cabin, was used to log the aircraft's position every one second. Using this device, the highest position accuracy achievable is ± 3 m, although this information is not logged. The images collected were checked for quality before being processed in AgiSoft Metashape Professional to create an orthomosaic and a digital surface model (DSM) with 50 cm horizontal resolutions. Reports of topographic change after the eruption were also made available via the bulletin reports of the Smithsonian Global Volcanism Program (Global Volcanism Program, 2021). In both cases, the variety of methods used and long time between measurements illustrates the challenges associated with acquiring topographic measurements at high relief, frequently erupting volcanoes.

3.2. TanDEM-X data processing

Interferometric processing of the TanDEM-X CoSSC data was performed with the GAMMA InSAR processing software (GAMMA Remote Sensing AG), Werner et al. (2000). The process can be split into 3 main blocks: (1) Processing of the Single Look Complex (SLC) image pair and generation of initial interferogram; (2) Simulation of topographic phase based on a pre-existing, pre-eruptive DEM and removal of said topographic phase so as to generate a differential interferogram with fringes corresponding solely to the difference between the CoSSC-measured topography and the pre-eruptive DEM topography; (3) Unwrapping of the interferogram, height map generation and DEM geocoding. This process is illustrated in the block diagram shown in Fig. 3. Further post-processing for data visualisation and quality masking of the generated DEM/height maps was carried out in MATLAB.

Multilooking in the azimuth and range dimensions is performed so that the pixel spacing of the image products are brought closer to the pixel spacing of the DEM used, and also as close as possible to square pixels (i.e. approximately equal spacing in range and azimuth). This holds for both the interferogram generation itself, as well as for the separate multilooking of the images that is required as part of the process of geocoding the pre-existing DEM to radar geometry for the removal of topographic phase. For the El Reventador TDX data, this was 5 looks in range and 3 in azimuth for a resolution close to matching the upsampled SRTM 6 m DEM while for the La Soufrière, St. Vincent TDX data multilooking was 2 looks in range and 1 in azimuth for a resolution as close as possible to the Pléiades 2 m DEM.

The resulting interferograms typically include a large numbers of closely packed fringes due to the steep topography, making direct interferogram unwrapping unfeasible. This is a commonly encountered problem in volcanic environments; removing the topography's contribution to the interferogram phase can greatly assist with unwrapping. This is facilitated via the use of a pre-existing, pre-eruptive DEM from which the effect of topography can be modelled and subsequently subtracted from the interferogram prior to unwrapping. This process relies on accurate co-registration of the SAR images to the DEM, which required manual initial offset estimation correction for some experimental TDX CoSSC products; more information on said process, as well as the produced offsets between DEM and SAR imagery is available as Supplementary Material to this paper.

Table 2
Range bandwidth, Azimuth bandwidth and Pulse Repetition Frequency values relevant to the sub-sampling process for TanDEM-X and Harmony/Sentinel-1.

Radar parameter	TDX	HRM
Range bandwidth	100 MHz	56.5 MHz
Azimuth bandwidth	2765 Hz	320 Hz
PRF	3599 Hz	1717 Hz

After the topographic phase has been removed, the interferograms are flattened, filtered and unwrapped using the Minimum Cost Flow algorithm (MCF) (Eineder et al., 1998). Converting the unwrapped interferogram into a height change map requires as accurate as possible an estimate of the baseline geometry. Any inaccuracies in the orbital information of the SAR products can lead to inaccurate estimation of the baseline geometry; baseline estimates are refined using manually selected ground control points where no topographic change is known to have taken place.

3.3. Synthetic Harmony data

The spatial resolution of TanDEM-X images (3 m, with pixel spacings of 1–2 m; Table 1) is much finer than the spatial resolution of Harmony, which is inherently tied to Sentinel-1 spatial resolution of ~20 m. In the interest of gaining some insight into Harmony's observational capabilities, we seek here to simulate this lower spatial resolution. Rather than simply subsampling the topographic change maps, we sub-sample the original TDX SLC data and reprocess them. We do this in the frequency domain; the image spectrum is obtained via a Fast Fourier Transform (FFT) and is then appropriately decimated to reduce the spatial resolution of the image down to 20 m × 5 m (Fig. 4). This avoids the aliasing effects of direct spatial-domain subsampling (e.g. by multilooking or averaging the SLC data) and allows us to investigate the effect of the lower spatial resolution on the InSAR processing chain itself, in particular the challenge of phase unwrapping.

The spatial resolution of the two platforms can be related to each other in terms of bandwidth. For the range dimension of the simulated Harmony images we aim to retain a number of samples N_{rg}^{HRM} such that:

$$N_{rg}^{HRM} = B_{rg}^{HRM} \frac{N_{rg}^{TDX}}{f_s^{TDX}} \tag{1}$$

where B_{rg}^{HRM} is the range bandwidth of Harmony, N_{rg}^{TDX} is the number of original TDX range samples in the FFT and f_s^{TDX} is the range sampling frequency of the TDX data. In the azimuth direction, the number of azimuth samples to retain (N_{az}^{HRM}) is given by:

$$N_{az}^{HRM} = B_{az}^{HRM} \frac{N_{az}^{TDX}}{PRF^{TDX}} \tag{2}$$

where B_{az}^{TDX} is the azimuth processing bandwidth of Harmony, N_{az}^{TDX} is the number of original (TDX) azimuth samples in the FFT and PRF^{TDX} is the Pulse Repetition Frequency (PRF) for the TDX CoSSC product. The azimuth sampling rate (in seconds) Δt is equal to the inverse of the PRF for data in Stripmap mode. Table 2 gives the relevant parameter values for TanDEM-X and Harmony (whose radar parameters are dictated by Sentinel-1).

We bring the TDX data to ≈ 20 m × 5 m resolution matching that of Sentinel-1 imagery, which in the interferometric processing is then brought to the ≈ 20 m × 20 m resolution of Harmony products (e.g. by taking 4 looks in the range direction). These 20 m sub-sampled versions of the SLC data are referred to as HRM data in the remainder of the manuscript.

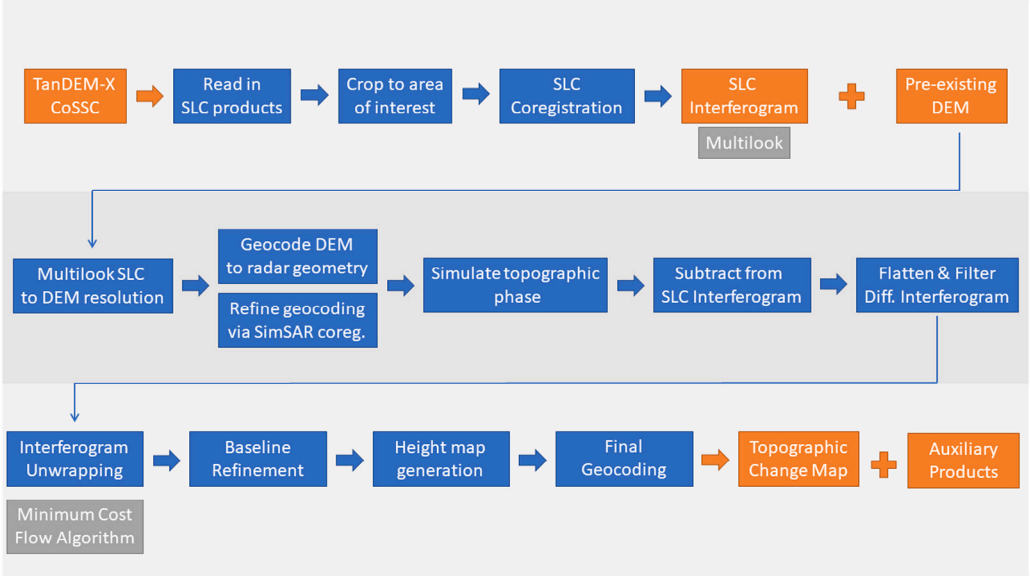

Fig. 3. Block diagram of the GAMMA processing steps for the interferogram generation, topographic phase removal and differential height map generation procedures.

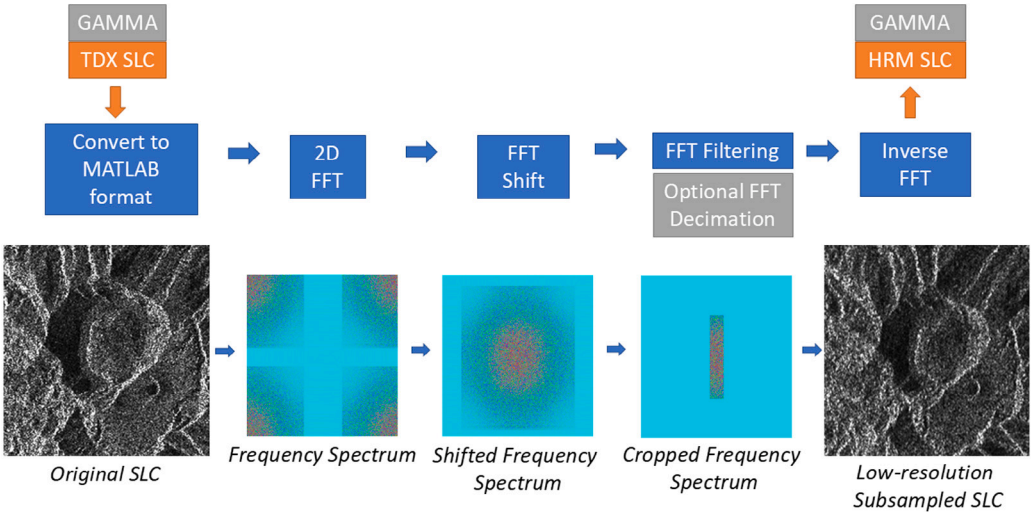

Fig. 4. Frequency domain subsampling of TDX SLC to HRM SLC.

3.4. Resolution and precision

The ability to resolve topographic change is limited by (1) the spatial resolution, which is a function of the local viewing geometry, and (2) vertical precision, which depends on the perpendicular baseline and radar coherence (Albino et al., 2020). Here we use radar system parameters and local topography to create maps of precision and resolution that can be used to mask out areas of low quality across the topographic change map. This enables us to identify the cause of any erroneous measurements and removes them from future calculations.

The optimal ground resolution δ_{gr} is a function of the radar viewing geometry and can be given by:

$$\delta_{gr} = \frac{\delta_{sr}}{\sin\theta} \tag{3}$$

where δ_{sr} is the slant-range pixel spacing and θ is the local incidence angle (Hanssen, 2001). While the incidence angle to the centre of the scene (typically provided as part of SAR metadata) can be used here, it is a very crude approximation of the real world local incidence angle as that varies throughout the scene, both from near- to far-range across the imaged area, and also in relation to the local topography. The orientation of the terrain slope with respect to the satellite's line of sight directly affects the ground resolution. In practice, this means one flank of the volcano will be imaged with optimal resolution for any given pass, illustrating the need for both ascending and descending acquisitions over volcanoes (e.g. Ebmeier et al., 2013). We therefore opt to produce local incidence angle maps accounting for the effect of topography as described by a DEM (either pre-eruptive DEM in the case of pre-eruptive data or a combination of pre-eruptive DEM updated with measured post-eruptive topographic change in cases of severe change in the landscape). Such local incidence angle maps can be produced as standard outputs of various interferometric SAR toolboxes such as GAMMA; gridding artefacts may however arise as a result of the resampling/reprojecting operations that are required to determine the DEM in the radar viewing geometry. Where such adverse effects were observed, we apply a simple low-pass Gaussian filter to the local incidence angle map.

The vertical precision σ_z of InSAR-derived DEMs is correlated with the SAR geometry and coherence values of the interferogram. It can be approximated using the following formula (Krieger et al., 2007)

$$\sigma_z = \frac{H_a}{2\pi}\sigma_\phi \tag{4}$$

where H_a is the Height of Ambiguity and σ_ϕ is the standard deviation of the phase. In turn, H_a can be calculated as

$$H_a = \frac{\lambda R \sin\theta}{B} \tag{5}$$

where λ is the radar wavelength, R is the slant range, θ is again the local incidence angle and B is the perpendicular baseline. Note that both Eqs. (4) and (5) are specific to the case of bistatic radar; the equivalent for mono-static would differ by a factor of two at the denominator. The standard deviation of the phase σ_ϕ can be approximated by the Cramér-Rao bound as

$$\sigma_\phi = \sqrt{\frac{1-\gamma^2}{2N\gamma^2}} \tag{6}$$

where γ is the coherence value and N is the number of looks.

While the wavelength and a number of other system parameters differ between the TanDEM-X and Harmony missions, the coherence of both is expected to be comparable; for the purposes of our experiments we assume the coherence maps for both TDX and HRM to be the same.

Qualitative masking of the DEM can be performed on the basis of these two measures, ground resolution δ_{gr} and vertical precision σ_z. If any pixel point in the scene exhibits δ_{gr} or σ_z exceeding a desired threshold it can then be considered unreliable and be masked out, with its value excluded and/or amended for future calculations/processing steps. Both δ_{gr} and σ_z are measured in meters, and a suitable threshold for each is best arrived at experimentally. Depending on the application at hand, working with a masked out TOC map may be sufficient and/or preferable. However, measurements such as the calculation of total extruded volumes or averages of topographic change within regions of interest (e.g. a lava dome or tephra deposit field) may be significantly skewed if pixels within those regions are completely excluded from the calculations due to the masking process. For such calculations we use a version of the TOC map where masked-out pixels are inpainted via a linear interpolation method (D'Errico, 2024).

4. Results

4.1. TanDEM-X

4.1.1. Lava flow field at El Reventador, Ecuador

Fig. 5 shows maps of SAR backscatter, resolution, precision and topographic change in the lava flow field of El Reventador, Ecuador generated using TanDEM-X. Local incidence angle calculations take into account the topographic change due to the deposition of lava flows and the growth of the cinder cone in the years after the SRTM mission acquisition. The resolution map (Fig. 5b) shows high values (i.e. poor resolution) on west facing slopes, while the precision map (Fig. 5c) shows high values (i.e. poor precision) on the steep eastward facing slopes that are in radar shadow and hence have poor coherence. The topographic change map from September 2011 (taken with SRTM as the reference) clearly shows positive and negative height changes associated with volcanic processes. However, there is significant noise on the steep slopes and we use the resolution and precision maps to mask low quality areas in subsequent topographic change maps (Fig. 6). Based on visual inspection, we set the masking thresholds to 12 m for vertical precision and 9 m for spatial resolution.

Fig. 6 shows masked topographic change maps from both the 2011 and 2014 TanDEM-X interferograms relative to SRTM as well as the differential topographic change from 2011 to 2014, with the corresponding lava flow fields demarcated as per Naranjo et al. (2016) and Arnold et al. (2017). The 2000–2011 map shows a large area of deposited material to the southeastern flank of the volcano, along with an area of removed material (negative elevation change) on the volcano summit (Fig. 6a). These correspond to the lava flow field deposited from 2002–2009 and to the removal of material from the summit during the subplinial eruption of November 2002 respectively (Arnold et al., 2017). Between September 2011 to June 2014, additional lava flows led to the deposit of material that largely filled the summit crater, as well as to additional flow field deposits to the north, northeast and directly east of the summit (Fig. 6b,c). Note that as the latest data is from 2014, the later lava flow field is not fully present yet.

4.1.2. Explosive eruption of La Soufrière, St Vincent

For the explosive eruption of La Soufrière, St Vincent, we processed and analysed the 3 TanDEM-X products available (Table 1). The availability of both ascending and descending pass of pre-eruptive data over La Soufrière, St. Vincent, provides an opportunity to evaluate the effect of pass direction on the ground resolution, vertical precision and the produced height change maps. Fig. 7 illustrates the difference in look direction, with its effect primarily noticeable in the maps of ground resolution. The ascending pass acquisition has low resolution on the eastern side of the volcano crater (larger values of spatial resolution), whereas the descending pass exhibits a similar situation on the western flank of the volcano. This illustrates that in areas of very steep topography it is highly desirable that data from both ascending and descending orbits are available, as the potential topographic change of interest may well be discernible on only one of the two, based on its location relative to the imaging geometry; numerous examples of such cases can be found in the literature (Galetto et al., 2024; Kubanek et al., 2021).

No significant topographic change is expected to be present in either of the two pre-eruptive interferograms, which should be in good agreement with the underlying pre-eruptive Pléiades DEM. However, Fig. 7(d) and (h) both show large measurements (up to 60 m positive and negative topographic change for the January 2017 data and −70 m for March 2019) to the east of the crater, where the precision maps (Fig. 7(c) and (g)) also show very large values. The original SAR images (shown geocoded in Fig. 7a and e) show foreshortening in the ascending and shadow in the descending pass, which will lead to poor coherence. Additionally, this region overlaps with part of the underlying Pléiades DEM that was infilled with upsampled SRTM data due to cloud coverage, which may have further caused artefacts in the geocoded SAR images. This reinforces the argument for masking of the produced DEMs in the interest of eliminating such areas of erroneous measurements. Examples of such masking can be seen in subsequent figures (e.g. in Fig. 8c we set masking thresholds at 4 m for resolution and 10 m for precision), resulting in the majority of such erroneous measurement pixels being masked out.

The eruption caused significant changes in the topography of the crater and the surrounding area; these are visually evident in Fig. 8 which shows both pre-eruptive and post-eruptive SAR backscatter images as well as the generated topographic change map from the October 2021 acquisition. The 1979 dome can be clearly seen in the 2017 pre-eruptive SAR image, though the newer 2020–2021 dome is obviously not yet present by this point. The post-eruptive data show the significant changes in the crater, which are consistent with other reports about the eruption (Joseph et al., 2022; Global Volcanism Program, 2021). The 1979 and 2020–2021 lava domes were completely destroyed, and in their position is a new, smaller crater about 800 m in diameter, while deposits of tephra are present along the eastern side of the crater, with two significant deposits of tephra located at the edges of the tephra field north and south of the newly formed crater. The topographic change map constructed from TanDEM-X data shows change consistent with this overall picture, with both the new crater and tephra deposits clearly present.

4.2. Simulated Harmony data

4.2.1. Lava flow field at El Reventador, Ecuador

Fig. 9 shows measurements of topographic change over El Reventador lava flow field from September 2011 to July 2014 created using our simulated HRM data. Outputs are geocoded to the up-sampled 6 m SRTM DEM. To assess the precision, we use a fixed baseline value

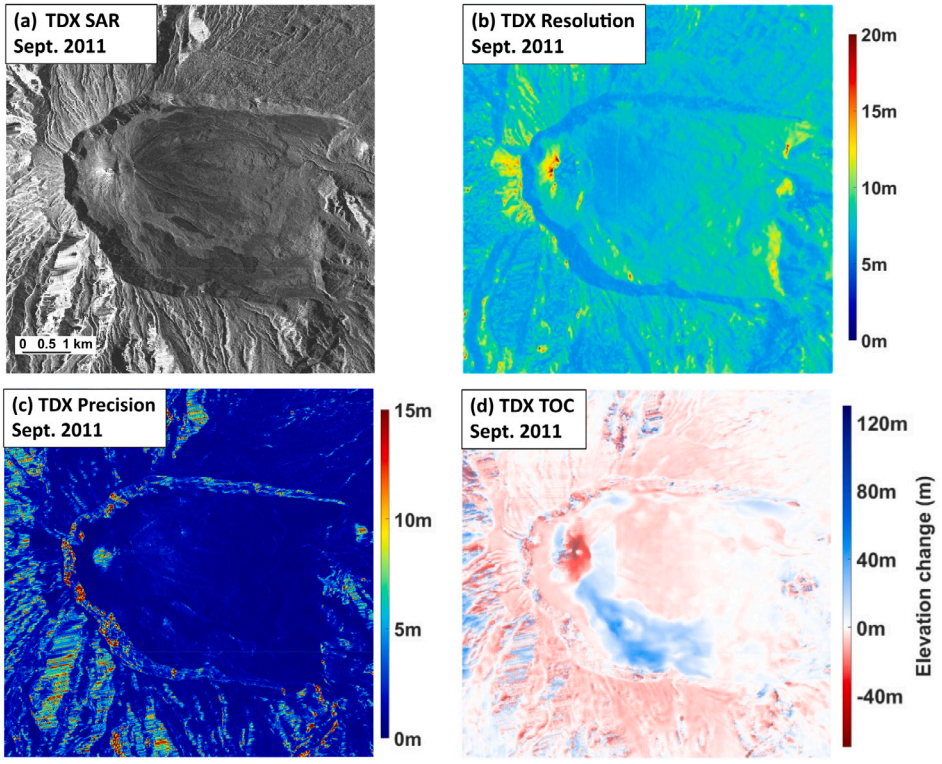

Fig. 5. TanDEM-X measurements of the lava flow field at El Reventador, Ecuador. (a) TDX SAR Image acquired in September 2011 (ascending). (b) Ground Resolution map. (c) Precision map. (d) Topographic change between the TanDEM-X acquisition in September 2011 and SRTM DEM acquired in 2000.

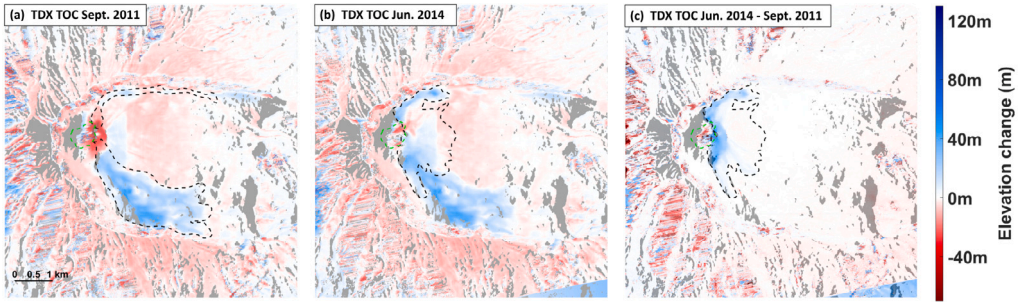

Fig. 6. TanDEM-X topographic maps of the lava flow field at El Reventador, Ecuador (a) Topographic change map using September 2011 TDX data relative to SRTM topography (acquired in 2000). Lava flow field from 2002–2009 demarcated as per Naranjo et al. (2016) in dashed black line. (b) Topographic change map using June 2014 TDX data relative to SRTM topography (acquired in 2000). Lava flow field from 2011–2016 demarcated as per Arnold et al. (2017) in dashed black line. (c) Differential topographic change map using June 2014 TDX data relative to the SRTM DEM as updated according to the September 2011 measured topographic change, effectively showing only the topographic change occurring between September 2011 and June 2014. Lava flow field from 2011–2016 demarcated as per Arnold et al. (2017) in dashed black line. Summit area outlined in dashed green line. Grey pixels are masked at 9 m resolution and 12 m precision.

of 630 m based on Harmony's current mission plan (ESA Harmony Mission Advisory Group, 2022; ESA Earth and Mission Science Division, 2023) for El Reventador's latitude, rather than maps of the estimated perpendicular baseline that were available for TanDEM-X. The wavelength λ has also been changed to the Sentinel-1 equivalent value of 5.54 cm. We use the coherence maps from TanDEM-X which we assume to be comparable to that achievable by Harmony. We set masking thresholds at 36 m vertical accuracy and 40 m spatial resolution (twice the nominal 20 m resolution of Harmony).

The HRM images of topographic change appear very similar to that of the original TDX data previously shown in Fig. 5 and we perform a quantitative comparison of the estimates of total lava flow volume and summit elevation (Table 3). In order to quantify the uncertainty inherent in our measurements of lava flow volumes and summit height, we have used the standard deviation of measurements within the reference area shown in Fig. 2. In this area we expect little to no topographic change to have occurred, and we corroborate this by noting a sub-1 m mean change across the area. We calculate the standard deviation of both the September 2011 and June 2014 TDX data at 1.35 m, whereas the HRM data have a lower standard deviation of 0.65 m on September 2011 and 0.9 m on June 2014; this makes us confident that we can detect topographic change of over 1.4 m at all cases. We use this value of 1.4 m as a confidence interval for our measurements of height and volume (accounting for a volume change of ± this height value at every pixel in the region of interest). These intervals are noted in the results shown in Table 3. For these measurements, we only take into account pixels of positive topographic change within the outlines of each lava flow (shown in Fig. 6); i.e. small areas of negative topographic change within the flows (corresponding to material removed from the summit during the explosive part of the eruption) are treated as zero-valued.

Measurements using the TDX data from September 2011 show a total volume of 84.6 ± 5.8 × 10^6 m^3 of deposited material inside the area of the 2002–2009 lava flow field relative to SRTM; using the corresponding HRM data the deposited volume measures at 91.6 ± 5.8

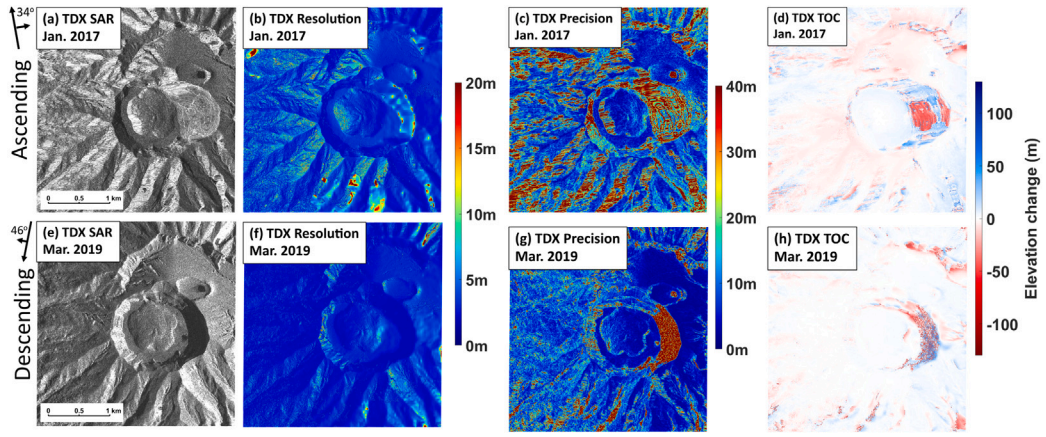

Fig. 7. Demonstration of the effect of pass direction on Ground Resolution and Precision.(a), (e) SAR Image of La Soufrière, St. Vincent, acquired in January 2017 (pre-eruption, ascending) and March 2019 (pre-eruption, descending) respectively. (b), (f) Ground Resolution map. (c), (g) Precision map. (d), (h) Topographic change map.

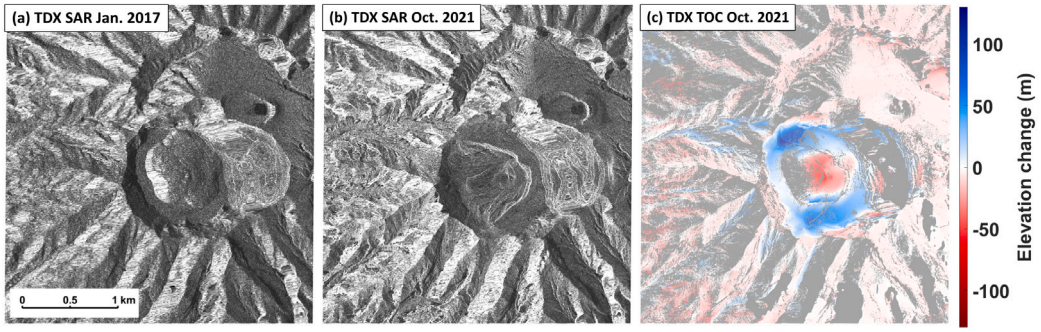

Fig. 8. Topographic change after the eruption of La Soufrière, St. Vincent.(a) TDX SAR Image acquired in January 2017 (pre-eruption, ascending), (b) TDX SAR Image acquired in October 2021 (post-eruption, ascending), and (c) masked post-eruptive topographic change map using October 2021 data.

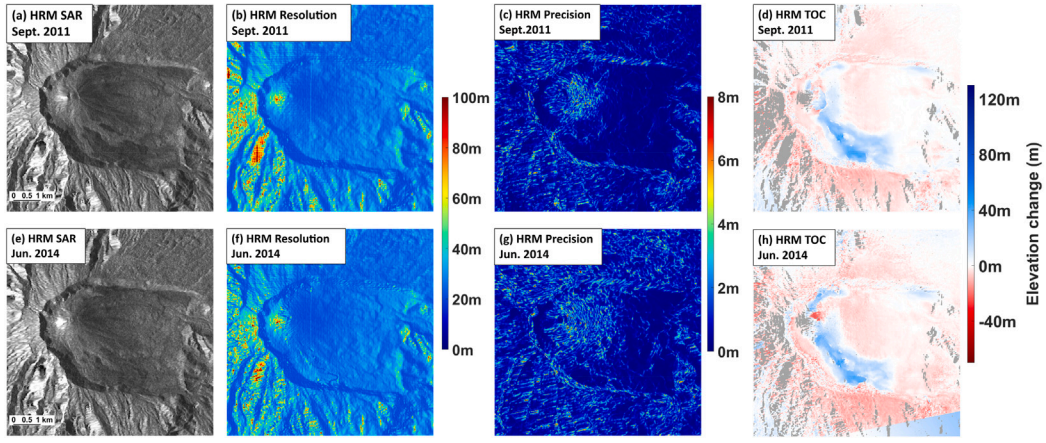

Fig. 9. Topographic change of evolving lava flows in El Reventador (a), (e) HRM SAR Image acquired in September 2011 (ascending) and July 2014 (ascending) respectively. (b), (f) Ground Resolution map. (c), (g) Precision map. (d), (h) Masked Height change map. Masking thresholds at 40 m for resolution and 36 m for precision. Topographic change relative to SRTM DEM.

$\times 10^6$ m^3. Both these values are close to the planimetric estimation of total flow volume of 90×10^6 m^3 reported in Naranjo et al. (2016). TDX data from June 2014 show a total bulk volume increase of $32.9 \pm 3.9 \times 10^6$ m^3 in the area corresponding to the 2011–2016 lava flow field (measurement relative to SRTM), while HRM data measure at $34.6 \pm 3.9 \times 10^6$ m^3. Both measurement values are within the cumulative bulk volume difference of $33.3 \pm 1.5 \times 10^6$ m^3 reported in Arnold et al. (2017).

Vallejo et al. (2023) have extensively studied the morphology of the summit of El Reventador and its changes during the various eruptive phases from 2002 onwards and we compare their estimates of summit height to our measurements in Table 3. Vallejo et al. (2023) report that prior to the eruptive activity of 2002 El Reventador had a maximum height of 3560 m. Summit height was reduced to 3526 m due to the explosive eruption of 2002 and was then rebuilt during subsequent phases of the eruption, reaching a maximum height of approximately 3600 m, with measurements of 3545 m and 3546 m reported in October 2011 and October 2013 respectively (Vallejo et al., 2023). Our summit height measurements using InSAR data from September 2011 show a summit elevation of 3570 ± 1.4 m using TDX data and 3548 ± 1.4 m

Table 3
Measurements of topographic change in El Reventador using full resolution TanDEM-X and subsampled simulated Harmony data. Ground truth provided via Naranjo et al. (2016), Arnold et al. (2017) and Vallejo et al. (2023).

	TDX	HRM	Ground Truth
Lava flow '02-'09	$84.6 \pm 5.8 \times 10^6$ m^3	$91.6 \pm 5.8 \times 10^6$ m^3	90×10^6 m^3 (Naranjo et al., 2016)
Lava flow '11-'16	$32.9 \pm 3.9 \times 10^6$ m^3	$34.6 \pm 3.9 \times 10^6$ m^3	$33.3 \pm 1.5 \times 10^6$ m^3 (Arnold et al., 2017)
Summit Height '11	3570 ± 1.4 m	3548 ± 1.4 m	3545 m (Vallejo et al., 2023)
Summit Height '14	3543 ± 1.4 m	3547 ± 1.4 m	≈ 3546 m (Vallejo et al., 2023)

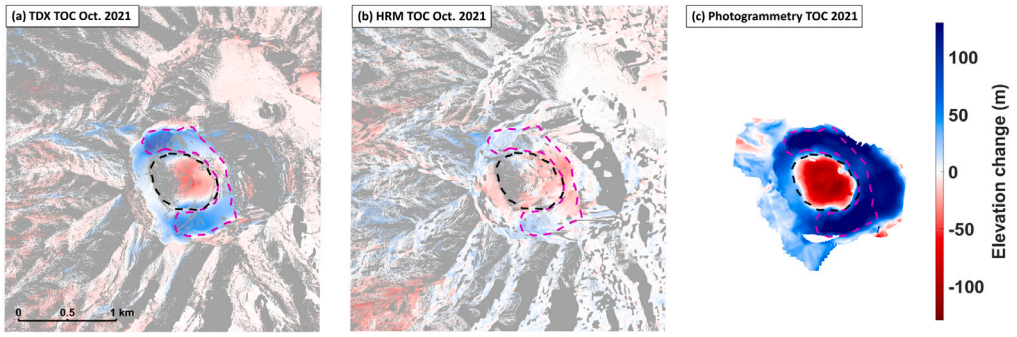

Fig. 10. Topographic change after the eruption of La Soufrière, St. Vincent. Topographic change maps generated from (a) TDX data and (b) HRM data. Masking via resolution and precision maps with resolution thresholds at 4 m and 40 m for TDX and HRM respectively, precision thresholds at 10 m and 25 m for TDX and HRM respectively. (c) Topographic change measured using photogrammetry. New crater area and tephra field deposits demarcated in dashed black and dashed magenta outlines respectively.

using HRM data. It is worth noting that in the case of the September 2011 TDX data there appear to be some outliers in the summit region which persist after masking, and which we have manually excluded. Conversely, measurements from June 2014 show a summit elevation of 3543 ± 1.4 m for TDX and 3547 ± 1.4 m for HRM. These values are close to those reported in Vallejo et al. (2023), more so than the summit height of 3355 m reported in Naranjo et al. (2016).

The close agreement of TanDEM-X, HRM and ground-truth measurements of lava flow volume and summit height for El Reventador, demonstrates the utility of bistatic radar systems. In this scenario, Harmony's lower resolution is not particularly detrimental, as the topographical change of interest can still be accurately measured. Small numerical differences between the TDX and HRM measured volumes can to a degree be expected due to the differences in Harmony's resolving capabilities (particularly in terms of spatial resolution) as well as possible differences in the masking process.

4.2.2. *Explosive eruption of La Soufrière, St Vincent*

We then measure topographic change for La Soufrière, St. Vincent using the corresponding sub-sampled HRM data. A fixed baseline value of 535 m was used for the ascending pass height of ambiguity calculations, again set according to current mission specifications for La Soufrière, St. Vincent's latitude. Masking was performed by thresholding at 25 m for vertical precision and 40 m for spatial resolution (twice the nominal 20 m resolution of the data). Fig. 10 presents a comparison between the TDX and HRM topographic change maps along with a topographic change map created by aerial photogrammetry that serves as ground truth. There is overall good alignment in the features present, as in an area of negative topographic change (corresponding to the new crater) with surrounding positive topographic change (corresponding to tephra deposits) can be clearly seen, but there are also significant discrepancies.

The differences between the TanDEM-X and photogrammetric change maps (Fig. 10) can be attributed to differences in referencing and acquisition timing. The photogrammetry-derived DEM from which the TOC map of Fig. 10c contains inaccuracies in its absolute elevation values that are inherent to the data collection method and need to be corrected empirically. Ground control points would have been necessary for further accuracy in registering absolute heights to sea surface level, however their placement was not practically feasible in this case. The low resolution of the GPS receiver onboard the helicopter was another source of possible errors in the accurate registration of the produced DEM. As a result, the photogrammetric TOC map contained a strong ramp signal, showing non-negligible topographic change outside of the area of interest of the volcano crater, where none should be present. We have attempted to correct for this ramp however we cannot be certain that all underlying measurement errors were completely eliminated in doing so.

Even once the ramp has been removed, the photogrammetry method shows more extreme values than the TanDEM-X map. This can be attributed to the difference in acquisition dates between the photogrammetry data (June 2021) and the InSAR data (October 2021). Features of topographic change do not necessarily remain static post eruption as gradual cooling leads to contraction as well as due to compaction over time (Wittmann et al., 2017). Non-consolidated tephra deposits are less structurally stable and can be reworked by environmental forces such as strong winds and rainfall for years subsequent to an eruption (Panebianco et al., 2017; Jones et al., 2017). We therefore consider it possible and rather probable that the topography of the tephra deposits around the crater of La Soufrière, St. Vincent changed in the months between June and October of 2021, especially as that period spans the wet season in the Caribbean. It is possible that some of the material forming the two major mounds at the North and South of the crater could have been removed, as well as that some removed material could have partially filled in the adjacent crater. This highlights the importance of the higher temporal resolution measurements that will be provided by the Harmony Mission.

As in the previous case study, we have measured the standard deviation of our TOC measurements in a relatively flat reference area northeast of the crater, as shown in Fig. 2(c). For our post-eruptive TOC maps this was 0.41 m for the TDX and 0.66 m for HRM; we are therefore confident we would have detected a topographic change of over 0.7 m at either case. We use this value of 0.7 m as a confidence interval for our measurements of height and volume (accounting for a volume change of +− this height value at every pixel in the region of interest).

We conduct a quantitative comparison, which while not in as close agreement as at El Reventador, still illustrates TanDEM-X's capability to measure topographic change in this scenario (Table 4). TDX data show a maximum crater depth of 74 ± 0.7 m, with a total crater volume of $5.3 \pm 0.2 \times 10^6$ m^3. Photogrammetry TOC shows a maximum crater depth of 118 m, with a total volume of 16×10^6 m^3. Measurements produced within the magenta tephra field outline of Fig. 10 show a

Table 4
Measurements of topographic change in La Soufrière, St. Vincent.

	TDX	HRM	Ground Truth
Crater depth (max.)	74 ± 0.7 m	42 ± 0.7 m	118 m
Crater depth (avg.)	26.5 ± 0.7 m	16 ± 0.7 m	64 m
Crater volume change	$-5.3 \pm 0.2 \times 10^6$ m^3	$-3.8 \pm 0.2 \times 10^6$ m^3	-16×10^6 m^3
Tephra height (max.)	134 ± 0.7 m	44 ± 0.7 m	172 m
Tephra height (avg.)	50 ± 0.7 m	13.5 ± 0.7 m	117 m
Tephra volume	$16 \pm 0.24 \times 10^6$ m^3	$2.7 \pm 0.24 \times 10^6$ m^3	40×10^6 m^3

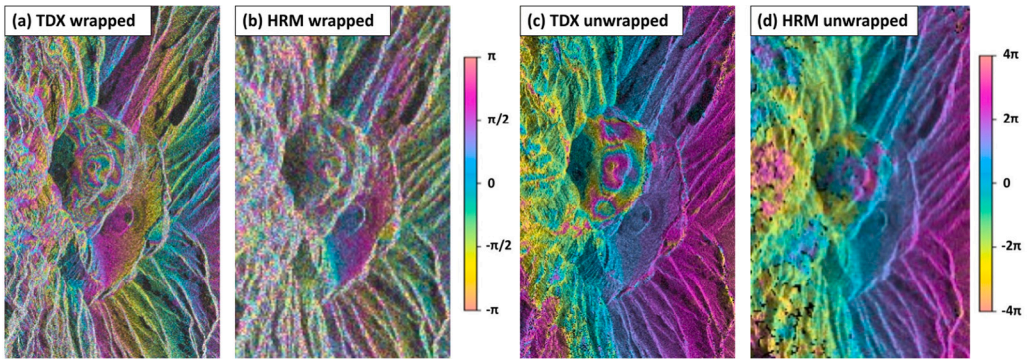

Fig. 11. Interferograms showing post-eruptive topographic change at La Soufrière, St. Vincent. (a) Wrapped phase TDX interferogram. (b) Wrapped phase HRM interferogram. (c) Unwrapped TDX interferogram. (d) Unwrapped HRM interferogram.

total tephra volume of $16 \pm 0.24 \times 10^6$ m^3 for the TDX data and 40×10^6 m^3 for the photogrammetry TOC, with a max height of 134 ± 0.7 m and 110 ± 0.7 m for the North and South tephra deposits respectively measured in the TDX data and corresponding heights of 172 m and 168 m measured in the photogrammetry TOC. It should be noted that the tephra field extends further to the east than the area outlined in magenta in Fig. 10, as can be seen in the photogrammetry TOC. We have opted here to perform our comparative calculations over this truncated subset so as to avoid measurements over a large masked region of poor-performing InSAR TOC maps.

The differences between the HRM TOC maps and the TDX TOC maps for La Soufrière, St. Vincent are significant (Fig. 10). There is some overall similarity in the pattern of topographic change, in that there is an area of negative topographic change (corresponding to the new crater) with surrounding positive topographic change (corresponding to tephra deposits). However, the area of negative topographic change is not only smaller than the ground-truth demarcated crater area but is also mis-aligned, appearing to be centred further east than expected. The tephra field appears different as well, with the two major tephra mounds still visible, albeit measuring at a much lower elevation, and a large part of the tephra field is dominated by negative topographic change, possibly due to the misplaced crater depression. The crater maximum depth is here measured at 42 ± 0.7 m, with a total volume of $3.8 \pm 0.2 \times 10^6$ m^3, while the tephra field measures at a total volume of $2.7 \pm 0.24 \times 10^6$ m^3, with a max height of 13.5 ± 0.7 m. Measurements of the maximum, average and estimated total volume of topographic change in the crater and tephra field using the various TOC maps can be found in Table 4.

While referencing issues and temporal variation may account for the differences between the TDX data and the photogrammetry DEM, these obviously do not apply in the case of the discrepancies between the TDX and HRM TOC. We attribute these to processing errors, primarily in the unwrapping of the produced interferogram. The steep topography of La Soufrière, St. Vincent presented a challenging scenario for unwrapping, particularly within in regions of very dense phase fringes around the summit corresponding to steep topographic change. The reduced spatial resolution of the HRM data has proven problematic in such areas, as it is not sufficient to resolve the closely packed fringes present in the interferogram; subsequently, the accuracy of topographic change measurements in such areas can deteriorate as demonstrated.

Fig. 11 shows examples of the post-eruptive wrapped and unwrapped interferograms for La Soufrière, St. Vincent, in both TDX and HRM resolutions. The deformation pattern corresponding to the new crater and the tephra deposits is clearly visible in the TDX unwrapped interferogram, however the HRM interferogram presents the issues discussed previously. Note that the interferograms are in radar viewing geometry and contain a ramp signal that was removed at a later processing stage.

We tested alternative approaches to improve unwrapping performance, but to little effect. Unwrapping using the GAMMA implementation of Branch Cut proved to be challenging even in the case of the full resolution TDX data. Additionally, attempts to unwrap using the new COMET LiCSAR unwrapper (Lazecky et al., 2022), which is based on snaphu with the addition of a number of pre-processing routines to improve performance, including filtering and phase gradient reduction, did not lead to any noticeable improvement. Finally, we did not notice any clear discontinuities in the wrapped interferogram that could be manually corrected.

5. Discussion

In the context of the scientific studies and mission design process for Harmony, we have performed a number of case studies on the use of bistatic InSAR for the measurement of volcanic topographic change with the aim of identifying some of the particular challenges associated with this observation scenario. The results presented here, particularly for the case of El Reventador demonstrate the great potential usefulness of a satellite mission such as Harmony being able to provide 20 m spatial resolution DEMs of evolving volcanoes at steady, frequent time intervals. The input of this case studies was communicated to ESA so as to inform mission design decisions related for example to the data acquisition strategy (ESA Earth and Mission Science Division, 2023).

5.1. Volcano monitoring

The availability of high resolution, up-to-date DEMs is of paramount importance to volcanology. Estimating the erupted mass provides the size of the eruption and eruptive rate (Galetto et al., 2023) and can be used to constrain physico-chemical models, providing estimates of magma compressibility and volatile content (Delgado et al., 2019; Yip

et al., 2022, 2024). Frequent measurements of topography can be used to identify changes in the extrusion rate, which can be indicative of upcoming changes in eruption characteristics. For example, Dualeh et al. (2023b) showed that the average extrusion rate of the lava dome at La Soufrière, St. Vincent was 1.8 m^3 s^{-1} between December 2020 and March 2021 but increased to 17.5 m^3 s^{-1} in the 2 days prior to the explosive eruption on 9 April 2021. Furthermore, rapidly changing topography can alter the trajectory of hazardous volcanic flows including lava flows, pyroclastic flows and lahars. Thus hazard assessments need to be continuously updated at erupting volcanoes, requiring up-to-date measurements of topography (Kubanek et al., 2021; Dzurisin et al., 2019).

However, often there are no pre- or post-eruptive DEMs, or the time of acquisition between two DEMs is large and therefore they cover multiple eruptions (Galetto et al., 2023). The regularity and temporal frequency of Harmony's planned acquisitions is therefore a key feature of the mission. DEMs generated from such data can help provide insightful timeseries into ongoing eruptions, at a time when monitoring via other means poses prohibitive dangers. However, as previously discussed, current bistatic InSAR missions are rarely able to provide high frequency acquisitions over volcanic regions; e.g. in the case of the recent La Soufrière, St. Vincent eruption studied here, no TDX acquisitions were available during the 6-month eruption period. This further reinforces Harmony stated aim of providing up-to-date DEMs over volcanic regions at a regular revisit rate of 12 days. Taking again the case of La Soufrière, St. Vincent, this would have furnished approximately 12 acquisitions over the period of December 2020 to June 2021, from which the evolution of the new lava dome as well as the effects of the explosive eruptive phase could have been assessed. Harmony's catalog of time series DEMs and topographic change maps is set to become an invaluable resource to the scientific community studying volcanoes and the devastating effects of their eruptions.

High resolution DEMs also serve as a basis for the estimation and subsequent removal of topographic phase, a crucial processing step when working with high resolution InSAR in areas of steep topography (Bemelmans et al., 2023; Muller et al., 2018). While high-resolution DEMs for a number of volcanoes have been developed over recent years (Dualeh et al., 2023b; Vallejo et al., 2023), this is unfortunately not always the case. For the case study on El Reventador, SRTM DEM data had to be upsampled to a higher resolution closer to that of the TDX data, so as to facilitate phase unwrapping (Arnold et al., 2017). While this upsampling strategy was viable in this case, it is far from optimal, and is reliant on little to no topographic change other than the one of interest having occurred since the acquisition of the reference DEM; a situation that will clearly not be the case over the passing of time.

5.2. Processing challenges

The case study of La Soufrière, St. Vincent illustrates the processing and unwrapping challenges posed by the steep terrain of volcanic regions. While the full resolution TanDEM-X products are able to accurately recreate the observed topographic change, the simulated Harmony products are not. To identify the cause of the problem, we compare our results with those of the end-to-end numerical simulator, HEEPS/Terra, which uses realistic forward models to simulate the various Harmony products (Prats et al., 2023; ESA Harmony Mission Advisory Group, 2022). HEEPS/Terra generates simulated Harmony co-registered SLC image pairs, from which higher-level products such as TOC can be further simulated and then evaluated in terms of accuracy and noise performance. We use the full resolution TDX TOC maps created in this study as ground-truth inputs of topographic change to HEEPS/Terra and compare the outputs to our HRM simulations.

Fig. 12 shows the ground truth TOC and the HEEPS/Terra retrieved TOC for La Soufrière, St. Vincent. The ground truth TOC here is derived from the TDX TOC of October 2021 described previously, where masked out pixels have been filled in using bilinear interpolation. It is immediately evident that the two TOC maps of Fig. 12 are in very close agreement, much closer than the TDX and HRM TOC maps of Fig. 8 are. No misalignment of the main features is present, nor is there any significant difference in the observed magnitudes. The mean measurement error in this case is 0.68 m, with a standard deviation of 0.51 m (measured throughout the entire scene).

There is a fundamental difference between HEEPS/Terra and the HRM simulations. In the case of our subsampled HRM data, processing of the interferometric SLC image pair is undertaken in exactly the same fashion as it would be in the case of real world data, in this case using the MCF algorithm within GAMMA RS (Eineder et al., 1998) for phase unwrapping. In the case of HEEPS/Terra, however, the unwrapping process is partially bypassed, as the desired unwrapped end phase is already known in the context of the end-to-end radar-level simulation. Therefore, unwrapping can be assumed to be almost perfect.

This demonstrates that the failure to accurately measure topographic change using the sub-sampled HRM data in the case of La Soufrière, St. Vincent is not due to any inherent incapability of Harmony's resolving power, as it is apparently capable of delineating such topographic change. Rather it further strengthens the argument that the errors present were caused due to unwrapping inaccuracies, exaggerated due to the lower spatial resolution, which as described would not have manifested in the case of the HEEPS/Terra simulation and its ideal unwrapping conditions.

Unfortunately, the scenario encountered in our case study of La Soufrière, St. Vincent is fairly common. Steep summit topography is a common feature of many volcanoes, and particularly stratovolcanoes, which in turn make up for a very substantial portion of the Earth's volcanoes. The challenges encountered here may therefore be common when studying such volcanoes.

While new unwrapping algorithms are still occasionally presented in the literature (e.g. Yu et al., 2019), and more recently utilising deep learning approaches (Zeyada et al., 2022; Zhang et al., 2023), few appear to have had any widespread adoption in the InSAR community beyond the classic MCF and Branch Cut algorithms (and variants thereof). More significant inroads have been made in 3-D unwrapping (Hooper and Zebker, 2007), where techniques such as loop closure (Maghsoudi et al., 2022) lead to significant performance improvement in unwrapping InSAR timeseries data, though these are obviously of little use with singular bi-static data acquisitions. To that effect, we believe that developing a new generation of unwrapping algorithms that can successfully deal with the challenges posed by such steep topography is an important topic for future research, and we hope to be able to contribute in that direction in future science studies for the Harmony mission.

6. Conclusions

In this paper, we discuss the use of multistatic InSAR in volcano monitoring, and demonstrate how high-resolution TanDEM-X bistatic InSAR data can be utilised to evaluate topographic change after volcanic eruptions. Additionally, we simulate lower-resolution data to gain insights into the performance of ESA's upcoming Harmony InSAR mission. We identify and discuss some of the particular challenges involved in InSAR volcano monitoring that relate to local topography and viewing angle, and demonstrate the importance of multi-directional, frequent acquisitions as well as the need for quantitative evaluation and masking of produced DEMs.

CRediT authorship contribution statement

Odysseas Pappas: Writing – review & editing, Writing – original draft, Visualization, Validation, Software, Methodology, Investigation, Funding acquisition, Formal analysis, Data curation, Conceptualization. **Juliet Biggs:** Writing – review & editing, Writing – original draft,

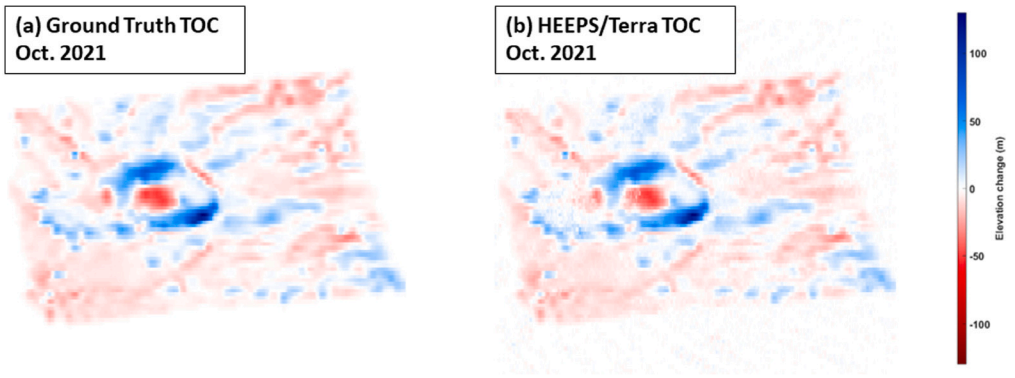

Fig. 12. Topographic change after the eruption of La Soufrière, St. Vincent as modelled by the DLR HEEPS/Terra simulator. (a) Topographic change as derived from the full-resolution TDX data of October 2021. (b) Simulated Harmony TOC measurement. Data shown in radar (slant range) viewing geometry.

Validation, Supervision, Resources, Methodology, Investigation, Funding acquisition, Formal analysis, Conceptualization. **Pau Prats-Iraola:** Writing – review & editing, Methodology, Investigation, Data curation. **Andrea Pulella:** Writing – review & editing, Investigation, Data curation. **Adam Stinton:** Writing – review & editing, Investigation, Data curation. **Alin Achim:** Writing – review & editing, Supervision, Resources, Funding acquisition.

Declaration of competing interest

The authors declare the following financial interests/personal relationships which may be considered as potential competing interests: Odysseas Pappas and Juliet Biggs report financial support was provided by Engineering and Physical Sciences Research Council. Odysseas Pappas and Juliet Biggs report financial support was provided by Natural Environment Research Council. Juliet Biggs and Pau Prats-Iraola report financial support was provided by European Space Agency. Juliet Biggs reports financial support was provided by European Research Council. If there are other authors, they declare that they have no known competing financial interests or personal relationships that could have appeared to influence the work reported in this paper.

Acknowledgements

We thank Jenni Barlcay and Paul Cole for discussions about the eruption of La Soufrière, St Vincent, and Paco Lopez Dekker and Björn Rommen for their discussions about the Harmony Mission.

Satellite data were provided through the Committee of Earth Observation Satellites (CEOS) Volcano Pilot for Disaster Risk Reduction, by Deutsches Zentrum für Luft- und Raumfahrt e.V. (DLR; German Aerospace Center) through proposal NTI_BIST7067. The photogrammetry data for La Soufrière, St Vincent was provided by the Montserrat Volcano Observatory under Data License DL-2024-01-Biggs.

PP and JB were supported by the European Space Agency, France under Contract 4000135083/21/NL/FF/ab, OP and JB were supported by an EPSRC IAA grant through the University of Bristol and COMET, the NERC Centre for the Observation and Modelling of Earthquakes, Volcanoes and Tectonics, a partnership between UK Universities and the British Geological Survey. JB received funding from the European Research Council (ERC) under the European Union's Horizon 2020 research and innovation programme (MAST; grant agreement No. 101003173).

Appendix A. Supplementary data

Supplementary material related to this article can be found online at https://doi.org/10.1016/j.rse.2024.114528.

Data availability

Data will be made available on request.

References

Abrams, M., Bailey, B., Tsu, H., Hato, M., 2010. The ASTER global DEM. Photogramm. Eng. Remote Sens. 76 (4), 344–348.

Albino, F., Biggs, J., Escobar-Wolf, R., Naismith, A., Watson, M., Phillips, J., Chigna Marroquin, G., 2020. Using TanDEM-X to measure pyroclastic flow source location, thickness and volume: Application to the 3rd June 2018 eruption of Fuego volcano, Guatemala. J. Volcanol. Geotherm. Res. 406, 107063. http://dx.doi.org/10.1016/j.jvolgeores.2020.107063.

Albino, F., Smets, B., d'Oreye, N., Kervyn, F., 2015. High-resolution TanDEM-X DEM: An accurate method to estimate lava flow volumes at Nyamulagira Volcano (D. R. Congo). J. Geophys. Res. 120 (6), 4189–4207. http://dx.doi.org/10.1002/2015JB011988.

Arnold, D.W.D., Biggs, J., Anderson, K., Vallejo Vargas, S., Wadge, G., Ebmeier, S.K., Naranjo, M.F., Mothes, P., 2017. Decaying lava extrusion rate at el Reventador Volcano, Ecuador, measured using high-resolution satellite radar. J. Geophys. Res. 122 (12), 9966–9988. http://dx.doi.org/10.1002/2017JB014580.

Arnold, D.W., Biggs, J., Dietterich, H.R., Vargas, S.V., Wadge, G., Mothes, P., 2019. Lava flow morphology at an erupting andesitic stratovolcano: a satellite perspective on El Reventador, Ecuador. J. Volcanol. Geotherm. Res. 372, 34–47. http://dx.doi.org/10.1016/j.jvolgeores.2019.01.009..

Bemelmans, M.J., Biggs, J., Poland, M., Wookey, J., Ebmeier, S., Diefenbach, A.K., Syahbana, D., 2023. High-resolution InSAR reveals localised pre-eruptive deformation inside the crater of Agung volcano, Indonesia. J. Geophys. Res. 128 (5), http://dx.doi.org/10.1029/2022JB025669.

Biggs, J., Wright, T.J., 2020. How satellite InSAR has grown from opportunistic science to routine monitoring over the last decade. Nature Commun. 11 (1), 3863. http://dx.doi.org/10.1038/s41467-020-17587-6.

Chorowicz, J., Deffontaines, B., Huaman-Rodrigo, D., Guillande, R., Leguern, F., Thouret, J., 1992. SPOT satellite monitoring of the eruption of Nevado Sabancaya volcano (Southern Peru). Remote Sens. Environ. 42 (1), 43–49. http://dx.doi.org/10.1016/0034-4257(92)90066-S.

Delgado, F., Kubanek, J., Anderson, K., Lundgren, P., Pritchard, M., 2019. Physico-chemical models of effusive rhyolitic eruptions constrained with InSAR and DEM data: A case study of the 2011–2012 Cordón Caulle eruption. Earth Planet. Sci. Lett. 524, 115736. http://dx.doi.org/10.1016/j.epsl.2019.115736.

D'Errico, J., 2024. Inpaint NaNs. MATLAB central file exchange. URL: www.mathworks.com/matlabcentral/fileexchange/4551-inpaint_nans, (Retrieved 29 January 2024).

Dirscherl, M., Rossi, C., 2018. Geomorphometric analysis of the 2014–2015 Bárdarbunga volcanic eruption, Iceland. Remote Sens. Environ. 204, 244–259. http://dx.doi.org/10.1016/j.rse.2017.10.027.

Dualeh, E., Ebmeier, S., Wright, T., Poland, M., Grandin, R., Stinton, A., Camejo-Harry, M., Esse, B., Burton, M., 2023a. Rapid pre-explosion increase in dome extrusion rate at La Soufrière, St. Vincent quantified from synthetic aperture radar backscatter. Earth Planet. Sci. Lett. 603, 117980. http://dx.doi.org/10.1016/j.epsl.2022.117980.

Dualeh, E., Ebmeier, S., Wright, T.J., Poland, M., Grandin, R., Stinton, A., Camejo-Harry, M., Esse, B., Burton, M., 2023b. Rapid pre-explosion increase in dome extrusion rate at La Soufrière, St. Vincent quantified from synthetic aperture radar backscatter. Earth Planet. Sci. Lett. 603, 117980. http://dx.doi.org/10.1016/j.epsl.2022.117980.

Dzurisin, D., Lu, Z., Poland, M.P., Wicks, Jr., C.W., 2019. Space-based imaging radar studies of US volcanoes. Front. Earth Sci. 6, 249. http://dx.doi.org/10.3389/feart.2018.00249.

Ebmeier, S.K., Biggs, J., Mather, T.A., Amelung, F., 2013. Applicability of InSAR to Tropical Volcanoes: Insights from Central America, vol. 380, Geological Society, London, Special Publications, pp. 15–37. http://dx.doi.org/10.1144/SP380.2, 1.

Ebmeier, S., Biggs, J., Mather, T., Elliott, J., Wadge, G., Amelung, F., 2012. Measuring large topographic change with InSAR: Lava thicknesses, extrusion rate and subsidence rate at Santiaguito volcano, Guatemala. Earth Planet. Sci. Lett. 335, 216–225. http://dx.doi.org/10.1016/j.epsl.2012.04.027.

Eiden, E., Pritchard, M.E., Lundgren, P.R., 2023. Spatial and temporal resolution needs for volcano topographic change data sets based on past eruptions (1980–2019). Earth Space Sci. 10 (10), e2023EA003054. http://dx.doi.org/10.1029/2023EA003054.

Eineder, M., Hubig, M., Milcke, B., 1998. Unwrapping large interferograms using the minimum cost flow algorithm. In: 1998 IEEE International Geoscience and Remote Sensing (IGARSS) Symposium Proceedings. vol. 1, pp. 83–87. http://dx.doi.org/10.1109/IGARSS.1998.702806.

ESA, 2019. Copernicus GLO-30 DEM. http://dx.doi.org/10.5270/ESA-c5d3d65.

ESA Earth and Mission Science Division, 2023. Earth Explorer 10 Mission Harmony - Mission Requirements Document. Technical Report.

ESA Harmony Mission Advisory Group, 2022. Earth Explorer 10 Candidate Mission Harmony: Report for Mission Selection. Technical Report.

Farr, T.G., Rosen, P.A., Caro, E., Crippen, R., Duren, R., Hensley, S., Kobrick, M., Paller, M., Rodriguez, E., Roth, L., Seal, D., Shaffer, S., Shimada, J., Umland, J., Werner, M., Oskin, M., Burbank, D., Alsdorf, D., 2007. The shuttle radar topography mission. Rev. Geophys. 45 (2), http://dx.doi.org/10.1029/2005RG000183.

Fiske, R.S., Sigurdsson, H., 1982. Soufrière volcano, St. Vincent: Observations of its 1979 eruption from the ground, aircraft, and satellites. Science 216 (4550), 1105–1106. http://dx.doi.org/10.1126/science.216.4550.1105.

Galetto, F., Dualeh, E., Delgado, F., Pritchard, M., Poland, M., Ebmeier, S., Shreve, T., Biggs, J., Hamling, I., Wauthier, C., Gonzalez Santana, J., Froger, J.-L., Bemelmans, M., 2024. The utility of TerraSAR-X, TanDEM-X, and PAZ for studying global volcanic activity: Successes, challenges, and future prospects. Volcanica 7 (1), 273–301. http://dx.doi.org/10.30909/vol.07.01.273301.

Galetto, F., Pritchard, M.E., Hornby, A.J., Gazel, E., Mahowald, N.M., 2023. Spatial and temporal quantification of subaerial volcanism from 1980 to 2019: Solid products, masses, and average eruptive rates. Rev. Geophys. 61 (1), e2022RG000783. http://dx.doi.org/10.1029/2022RG000783.

Global Volcanism Program, 2021. In: Bennis, K., Venzke, E. (Eds.), Report on Soufrière St. Vincent (Saint Vincent and the Grenadines). http://dx.doi.org/10.5479/si.GVP.BGVN202105-360150.

Grandin, R., Delorme, A., 2021. La Soufrière volcano (Saint Vincent) – fusion of pleiades (2014, 2 m) and copernicus (2018, 30 m) digital elevation models. http://dx.doi.org/10.5281/zenodo.4668734.

Grémion, S., Pinel, V., Shreve, T., Beauducel, F., Putra, R., Solikhin, A., Santoso, A.B., Humaida, H., 2023. Tracking the evolution of the summit lava dome of Merapi volcano between 2018 and 2019 using DEMs derived from TanDEM-X and Pléiades data. J. Volcanol. Geotherm. Res. 433, 107732. http://dx.doi.org/10.1016/j.jvolgeores.2022.107732.

Hanssen, R.F., 2001. Radar Interferometry: Data Interpretation and Error Analysis. Springer, http://dx.doi.org/10.1007/0-306-47633-9.

Hooper, A., Biggs, J., Yague-Martinez, N., Pinheiro, M., Prats, P., 2019. Harmony Phase-0 Science and Requirement Consolidation Study – Solid Earth - Technical Note on the Observation Scenarios, Performance Metrics and Performance Models. Technical Report HMNY-DLR-TN-01, DLR, University of Leeds, University of Bristol.

Hooper, A., Zebker, H.A., 2007. Phase unwrapping in three dimensions with application to InSAR time series. J. Opt. Soc. Amer. A 24 (9), 2737–2747. http://dx.doi.org/10.1364/JOSAA.24.002737.

Jones, R., Thomas, R.E., Peakall, J., Manville, V., 2017. Rainfall-runoff properties of tephra: Simulated effects of grain-size and antecedent rainfall. Geomorphology 282, 39–51. http://dx.doi.org/10.1016/j.geomorph.2016.12.023.

Joseph, E., Camejo-Harry, M., Christopher, T., Contreras-Arratia, R., Edwards, S., Graham, O., Johnson, M., Juman, A., Latchman, J., Lynch, L., Miller, V., Papadopoulos, I., Pascal, K., Robertson, R., Ryan, G., Stinton, A., Grandin, R., Hamling, I., Jo, M.-J., Barclay, J., Cole, P., Davies, B., Sparks, R., 2022. Responding to eruptive transitions during the 2020–2021 eruption of La Soufrière volcano, St. Vincent. Nature Commun. 13, 4129. http://dx.doi.org/10.1038/s41467-022-31901-4.

Kervyn, M., Ernst, G., Goossens, R., Jacobs, P., 2008. Mapping volcano topography with remote sensing: ASTER vs. SRTM. Int. J. Remote Sens. 29 (22), 6515–6538. http://dx.doi.org/10.1080/01431160802167949.

Krieger, G., Moreira, A., Fiedler, H., Hajnsek, I., Werner, M., Younis, M., Zink, M., 2007. TanDEM-X: A satellite formation for high-resolution SAR interferometry. IEEE Trans. Geosci. Remote Sens. 45 (11), 3317–3341. http://dx.doi.org/10.1109/TGRS.2007.900693.

Kubanek, J., Poland, M.P., Biggs, J., 2021. Applications of bistatic radar to volcano topography—A review of ten years of TanDEM-X. IEEE J. Sel. Top. Appl. Earth Obs. Remote Sens. 14, 3282–3302. http://dx.doi.org/10.1109/JSTARS.2021.3055653.

Kubanek, J., Richardson, J.A., Charbonnier, S.J., Connor, L.J., 2015a. Lava flow mapping and volume calculations for the 2012–2013 Tolbachik, Kamchatka, fissure eruption using bistatic TanDEM-X InSAR. Bull. Volcanol. 77 (12), 106. http://dx.doi.org/10.1007/s00445-015-0989-9.

Kubanek, J., Westerhaus, M., Heck, B., 2017. TanDEM-X time series analysis reveals lava flow volume and effusion rates of the 2012–2013 Tolbachik, Kamchatka fissure eruption. J. Geophys. Res. 122 (10), 7754–7774. http://dx.doi.org/10.1002/2017JB014309.

Kubanek, J., Westerhaus, M., Schenk, A., Aisyah, N., Brotopuspito, K.S., Heck, B., 2015b. Volumetric change quantification of the 2010 Merapi eruption using TanDEM-X InSAR. Remote Sens. Environ. 164, 16–25. http://dx.doi.org/10.1016/j.rse.2015.02.027.

Lazecky, M., Fang, J., Hooper, A., Wright, T., 2022. Improved phase unwrapping algorithm based on standard methods. In: IGARSS 2022 - 2022 IEEE International Geoscience and Remote Sensing Symposium. pp. 743–746. http://dx.doi.org/10.1109/IGARSS46834.2022.9884337.

Lopez-Dekker, P., Biggs, J., Chapron, B., Hooper, A., Kääb, A., Masina, S., Mouginot, J., Nardelli, B.B., Pasquero, C., Prats-Iraola, P., Rampal, P., Stroeve, J., Rommen, B., 2021. The harmony mission: End of phase-0 science overview. In: 2021 IEEE International Geoscience and Remote Sensing Symposium IGARSS. pp. 7752–7755. http://dx.doi.org/10.1109/IGARSS47720.2021.9554896.

Loughlin, S., Sparks, S., Brown, S., Jenkins, S., Vye-Brown, C. (Eds.), 2015. Global Volcanic Hazards and Risk. Cambridge University Press, http://dx.doi.org/10.1017/CBO9781316276273.

Maghsoudi, Y., Hooper, A.J., Wright, T.J., Lazecky, M., Ansari, H., 2022. Characterizing and correcting phase biases in short-term, multilooked interferograms. Remote Sens. Environ. 275, 113022. http://dx.doi.org/10.1016/j.rse.2022.113022.

McGuire, W.J., 1996. Volcano Instability: a Review of Contemporary Themes, vol. 110, Geological Society, London, Special Publications, pp. 1–23. http://dx.doi.org/10.1144/GSL.SP.1996.110.01.01, 1.

Mouginis-Mark, P.J., Rowland, S.K., Garbeil, H., Amelung, F., 2001. Topographic change on volcanoes from SRTM and other interferometric radars. In: IGARSS 2001. Scanning the Present and Resolving the Future. Proceedings. IEEE 2001 International Geoscience and Remote Sensing Symposium (Cat. No. 01CH37217). vol. 2, IEEE, pp. 757–758. http://dx.doi.org/10.1109/IGARSS.2001.976626.

Muller, C., Biggs, J., Ebmeier, S.K., Mothes, P., Palacios, P.B., Jarrín, P., Edmonds, M., Ruiz, M., 2018. Temporal evolution of the magmatic system at Tungurahua Volcano, Ecuador, detected by geodetic observations. J. Volcanol. Geotherm. Res. 368, 63–72. http://dx.doi.org/10.1016/j.jvolgeores.2018.11.004.

Naranjo, M.F., Ebmeier, S.K., Vallejo, S., Ramón, P., Mothes, P., Biggs, J., Herrera, F., 2016. Mapping and measuring lava volumes from 2002 to 2009 at El Reventador Volcano, Ecuador, from field measurements and satellite remote sensing. J. Appl. Volcanol. 5 (1), 8. http://dx.doi.org/10.1186/s13617-016-0048-z.

Panebianco, J., Mendez, M., Buschiazzo, D., Bran, D., Gaitán, J., 2017. Dynamics of volcanic ash remobilisation by wind through the Patagonian steppe after the eruption of Cordòn Caulle, 2011. Sci. Rep. 7, 45529. http://dx.doi.org/10.1038/srep45529.

Poland, M.P., 2014. Lava discharge rates determined from TanDEM-X imagery from Kīlauea Volcano, Hawai'i. In: 2014 IEEE Geoscience and Remote Sensing Symposium. pp. 3402–3405. http://dx.doi.org/10.1109/IGARSS.2014.6947211.

Poland, M.P., Zebker, H.A., 2022. Volcano geodesy using InSAR in 2020: the past and next decades. Bull. Volcanol. 84 (3), 27. http://dx.doi.org/10.1007/s00445-022-01531-1.

Porter, C., Howat, I., Husby, E., Noh, M.-J., Khuvis, S., Danish, E., Tomko, K., Gardiner, J., Negrete, A., Yadav, B., Klassen, J., Kelleher, C., Cloutier, M., Bakker, J., Enos, J., Arnold, G., Bauer, G., Morin, P., 2022. EarthDEM – Mosaics, version 1. Harv. Dataverse V1, http://dx.doi.org/10.7910/DVN/MVOWY7.

Porter, C., Howat, I., Noh, M.-J., Husby, E., Khuvis, S., Danish, E., Tomko, K., Gardiner, J., Negrete, A., Yadav, B., Klassen, J., Kelleher, C., Cloutier, M., Bakker, J., Enos, J., Arnold, G., Bauer, G., Morin, P., 2023. ArcticDEM – Mosaics, version 4.1. Harv. Dataverse V1, http://dx.doi.org/10.7910/DVN/3VDC4W.

Prats, P., Pulella, A., Benedikter, A., Hooper, A., Biggs, J., Kääb, A., Rabus, B., Nagler, T., Rott, H., Pappas, O., et al., 2023. Performance analysis of the harmony mission for land applications: Results from the phase A study. In: Fringe 2023. pp. 1–4.

Pritchard, M.E., Biggs, J., Wauthier, C., Sansosti, E., Arnold, D.W.D., Delgado, F., Ebmeier, S.K., Henderson, S.T., Stephens, K., Cooper, C., Wnuk, K., Amelung, F., Aguilar, V., Mothes, P., Macedo, O., Lara, L.E., Poland, M.P., Zoffoli, S., 2018. Towards coordinated regional multi-satellite InSAR volcano observations: results from the latin america pilot project. J. Appl. Volcanol. 7 (1), 5. http://dx.doi.org/10.1186/s13617-018-0074-0.

Shepherd, J., Aspinall, W., Rowley, K., Pereira, J., Sigurdsson, H., Fiske, R., Tomblin, J., 1979. The eruption of Soufrière volcano, St. Vincent April-June 1979. Nature 282 (5734), 24–28. http://dx.doi.org/10.1038/282024a0.

Stinton, A.J., 2024. Growth and Evolution of the Lava Dome and Coulée During the 2020–21 Eruption of la Soufrière, St Vincent, vol. 539, Geological Society, London, Special Publications, http://dx.doi.org/10.1144/sp539-2022-304.

Vallejo, S., Diefenbach, A., Gaunt, E., Almeida, M., Ramón, P., Naranjo, F., Kelfoun, K., 2023. 20 years of explosive-effusive activity at El Reventador volcano (Ecuador) recorded in its geomorphology. Front. Earth Sci. 11–2023, http://dx.doi.org/10.3389/feart.2023.1202285.

Werner, C., Wegmüller, U., Strozzi, T., Wiesmann, A., 2000. Gamma SAR and interferometric processing software. In: Proceedings of the Ers-Envisat Symposium, Gothenburg, Sweden. vol. 1620, Citeseer, p. 1620.

Wittmann, W., Sigmundsson, F., Dumont, S., Lavallèe, Y., 2017. Post-emplacement cooling and contraction of lava flows: InSAR observations and a thermal model for lava fields at Hekla volcano, Iceland. J. Geophys. Res. 122 (2), 946–965. http://dx.doi.org/10.1002/2016JB013444.

Yip, S.T.H., Biggs, J., Edmonds, M., Liggins, P., 2024. The role of pre-eruptive gas segregation on co-eruptive deformation and SO2 emissions. Earth Planet. Sci. Lett. 626, 118548. http://dx.doi.org/10.1016/j.epsl.2023.118548.

Yip, S.T.H., Biggs, J., Edmonds, M., Liggins, P., Shorttle, O., 2022. Contrasting volcanic deformation in arc and ocean island settings due to exsolution of magmatic water. Geochem. Geophys. Geosyst. 23 (7), e2022GC010387. http://dx.doi.org/10.1029/2022GC010387.

Yu, H., Lan, Y., Yuan, Z., Xu, J., Lee, H., 2019. Phase unwrapping in InSAR : A review. IEEE Geosci. Remote Sens. Mag. 7 (1), 40–58. http://dx.doi.org/10.1109/MGRS.2018.2873644.

Zeyada, H.H., Mostafa, M.S., Ezz, M.M., Nasr, A.H., Harb, H.M., 2022. Resolving phase unwrapping in interferometric synthetic aperture radar using deep recurrent residual U-net. Egypt. J. Remote Sens. Space Sci. 25 (1), 1–10. http://dx.doi.org/10.1016/j.ejrs.2021.12.001.

Zhang, L., Huang, G., Li, Y., Yang, S., Lu, L., Huo, W., 2023. A robust InSAR phase unwrapping method via improving the pix2pix network. Remote Sens. 15 (19), http://dx.doi.org/10.3390/rs15194885.